International Journal of Solids and Structures 48 (2011) 126–136

Contents lists available at ScienceDirect

International Journal of Solids and Structures

journal homepage: www.elsevier.com/locate/ijsolstr

Study of dynamic end effects in an elastic strip with sliding boundary conditions

Baruch Karp *

Department of Mechanical Engineering, Ben-Gurion University of the Negev, P.O. Box 653, Beer-Sheva 84105, Israel

ARTICLE INFO

Article history:
Received 31 March 2010
Received in revised form 11 August 2010
Available online 22 September 2010

Keywords:
Dynamic Saint-Venant's principle
Waveguide
Joints
SHM
End excitation

ABSTRACT

The dynamic response of an elastic, semi-infinite strip with sliding surfaces, subjected to various forms of end excitations, was solved analytically employing the property of bi-orthogonality of wave modes. An explicit relation between the amplitudes of evanescent waves and the form of the excitation was obtained. Quantitative measure for dynamic end effects was suggested, termed Saint-Venant ratio (SVR). It was shown that two qualities of that ratio are useful for monitoring the health of structural joints (SHM): being that ratio not affected by the intensity of the end excitation and its high sensitivity to small variations in the form of the excitation. The axial behavior of the strip subjected to several forms of end excitations was further used to demonstrate the validity of a previously suggested dynamic version of Saint-Venant's principle.

1. Introduction

Wave propagation and end effects are two phenomena typical to dynamic response of a semi-infinite waveguide. The characteristics of wave propagation are detailed well in several classical text books (e.g., Achenbach, 1973; Graff, 1975; Miklowitz, 1978). End effects, on the other hand, attracted less attention, with only general treatment in the text books. In particular, the closed form solution for waveguide response subjected to completely defined end excitations were suggested only in few studies (e.g., Gregory and Gladwell, 1984, 1989; Karp, 2008) with few more for a problem of end reflection (e.g., Torvik, 1967; Zemanek, 1972; Gregory and Gladwell, 1983). The present work belongs to that group of studies, with emphasis on end effects, represented by the evanescent waves.

The phenomenon of end effects in elastostatic problems is extensively investigated in many papers, commonly associated with Saint-Venant's principle (SVP). The phenomenon of dynamic end effects is also well understood, though the connection to SVP is less common. Recently, it was suggested to use both static and dynamic end effects as complimentary diagnostics for structural health monitoring (SHM) systems. In the study by Karp et al. (2008), the potential of such a method for monitoring the loosening of screws at a joint was experimentally demonstrated. In particular, small change in tightness level of each screw was easily detected by strain gauges located at the close vicinity to the end (near field) as compared to no change in reading of strain gauges located far from the end. Analytical studies of the effect of non-uniformity of end excitation are commonly limited to examination of the far-field response (see review by Karp, 2005, with recent results by Karp, 2008, 2009). Sensitivity of the near-field to the non-uniformity was investigated experimentally by Karp et al. (2008, 2009). Yet, analytical confirmation and explanation of the experimental results remain incomplete.

The main purpose of this paper is to provide a fundamental understanding for the experimental results related to the sensitivity of the near field to the form of the excitation. Emphasis is given to quantitative estimation of the phenomenon and to the possible usefulness of end effects as a structural signature for health monitoring of joints. The secondary objective is to illustrate the practical and theoretical aspects of dynamic Saint-Venant's principle (DSVP) as formulated in Karp (2009). These two aims are accomplished with the aid of analytical solution for the dynamic fields of an elastic, semi-infinite strip considered to be held in a plane strain condition with the lateral surfaces subjected to sliding conditions. These conditions, though not encountered in practice, admit an elegant mathematical solution without sacrificing much of the core behavior of waveguides.

Analytical solution for dynamic response of a plane waveguide with sliding surfaces is a standard introductory problem offered by any classical textbook on elastic waves (e.g., Miklowitz, 1978, Section 4.1; Graff, 1975, Section 8.1.2). Recent studies extend that analysis to a finitely pre-stretched strip (Karp and Durban, 2005; Wijeyewickrema et al., 2008). An extension of the analysis suggested here include formulae for coefficient analysis, enabling one to calculate the exact amplitudes of the wave modes for any given harmonic end excitation applied at the end of an elastic waveguide. The derivation suggested here closely follows the one

* Tel.: +972 86410694; fax: +972 86431291.
E-mail address: bkarp@bgu.ac.il

0020-7683/$ - see front matter © 2010 Elsevier Ltd. All rights reserved.
doi:10.1016/j.ijsolstr.2010.09.011

presented by Gregory and Gladwell (1984), and similar to that used by Rose (1999, p. 204). In these works, the derivation is limited to propagating modes in waveguide with free surfaces with no special attention to the evanescent waves. In the present study, evanescent modes are the main issue.

Calculation of amplitudes of propagating and evanescent waves is used to explicitly formulate surface strain generated by various forms of excitations. As a convenient quantitative measure of end effects, a ratio of the surface strain in the near field to the surface strain in the far field, termed Saint-Venant ratio (SVR), is introduced. The results expose high sensitivity of the SVR to the form of the excitation, suggesting that SVR is an effective structural signature of the form of the end data. That sensitivity renders the measurement of surface axial strain within the far- and the near-fields as an efficient method for identification of incipient changes in the details of end excitation. It is suggested that the analytical problem of semi-infinite strip subjected to end excitation can be considered to model an "active joint" connecting a beam-like (plate-like) component to a main structure. Then, measurement of SVR along the beam can be used as a complementary method to a structural health monitoring system, enabling detection of incipient damage at that joint.

In Section 2 the formulation of the problem of an elastic waveguide with sliding boundaries and its general solution is outlined. Formulae for amplitude of each mode are derived in Section 3. Several simple end excitations are solved explicitly in Section 4. In Section 5 few variations of a nominal excitation, resembling damaged joints, are worked out. A discussion of the results is given in Section 6.

2. A strip with sliding boundaries

Consider a semi-infinite strip with a thickness $2h$ made of homogeneous, isotropic, elastic material that occupies the region $x \geqslant 0$, $|y| \leqslant h$, $|z| < \infty$. The strip can be held in plane strain condition (the z coordinate not active) while the faces $y = \pm h$, $x \geqslant 0$, $|z| < \infty$ are sliding: zero tangential traction $\tau_{xy} = 0$ and zero normal displacement $u_y = 0$. At the end $x = 0$, a harmonic and symmetric (with reference to the x–z plane) excitation is applied with a circular frequency ω

$$\begin{aligned} &\sigma_x^0 = A_0 \mu \mathbb{S}(y) e^{-i\omega t}, \\ &u_y^0 = 0, \end{aligned} \quad \text{on } x = 0, \tag{1}$$

where σ_x^0, u_y^0 are the axial traction and the transversal displacement at the end, respectively, $\mathbb{S}(y)$ is the form of the excitation, μ is the shear modulus, and A_0 is the amplitude of the excitation (the real part of the expression is understood throughout the paper). The mixed nature of this boundary data is noted.

The dynamic response of a strip is governed by Navier's equation of motion

$$(\lambda + \mu)\nabla(\nabla \cdot \boldsymbol{u}) + \mu \nabla^2 \boldsymbol{u} = \rho \ddot{\boldsymbol{u}}, \tag{2}$$

where λ, μ are the Lame constants, ρ is the mass density, ∇ is the gradient vector and $\boldsymbol{u}$ is the displacement vector which has two components

$$\boldsymbol{u} = u_x \mathbf{i} + u_y \mathbf{j}, \tag{3}$$

for the two dimensional problem posed where both components u_x, u_y depend only on x and y coordinates and time, t. Here $\mathbf{i}$, $\mathbf{j}$ are the unit vectors in the x, y directions, respectively.

General solution to the stated problem is given in the form of separation of variables

$$\boldsymbol{u}(x, y, t) = \boldsymbol{U}(y) e^{i(\xi x - \omega t)} \tag{4}$$

with

$$\boldsymbol{U}(y) = U_x(y)\mathbf{i} + U_y(y)\mathbf{j}.$$

Here ξ is the *wave number*, $\boldsymbol{U}(y)$ is the associated cross-sectional profile for both displacement components (*wave mode*). The main steps of the derivation of the solution are recapitulated here (after Achenbach, 1973) with non-dimensional terms to be used hereafter, defined in Appendix A.

Imposing sliding conditions on the long faces

$$u_y = \tau_{xy} = 0, \quad \text{on } y = \pm h, \tag{5}$$

leads to two sets of uncoupled equations for symmetric and for anti-symmetric fields. For the sake of simplicity, we discuss here only symmetric fields. A non-trivial solution for the two amplitudes associated with symmetric fields (B and C in (A.3)) is obtained from the frequency equation (Achenbach, 1973)

$$\left[-2\xi^2 + (\xi^2 - \delta^2)\right] Sin(\gamma h) Sin(\delta h) = 0, \tag{6}$$

where γ, δ are defined in Eq. (A.4) in Appendix A.

Three conditions can individually fulfill Eq. (6)

$$(\xi^2 + \delta^2) = 0, \quad Sin(\gamma h) = 0, \quad Sin(\delta h) = 0. \tag{7}$$

The first of (7) requires $\omega = 0$ and bears no special interest in our context. The second and the third can be rewritten in an algebraic form

$$Sin(\gamma h) = 0 \Rightarrow \gamma_m = \frac{\pi}{2h} m, \quad m = 0, 2, 4, 6, \ldots, \tag{8}$$

$$Sin(\delta h) = 0 \Rightarrow \delta_n = \frac{\pi}{2h} n, \quad n = 2, 4, 6, \ldots. \tag{9}$$

By using the non-dimensional quantities defined in (A.9), these relations (8) and (9) between the wave number k and the frequency Ω become

$$k_m = \sqrt{\frac{\Omega^2}{\kappa^2} - m^2}, \quad m = 0, 2, 4, 6, \ldots \tag{10}$$

and

$$k_n = \sqrt{\Omega^2 - n^2}, \quad n = 2, 4, 6, \ldots \tag{11}$$

with κ defined in (A.9), m and n are non-dimensional wave numbers associated with dilatational and equivoluminal (shear, distortional) modes, respectively. An important consequence of the solutions (8) and (9) is that the roots k_m and k_n are discrete and take values either real or purely imaginary. For a given frequency ω in (1), Eq. (6) can be fulfilled by real or imaginary wave numbers ξ. Real wave numbers represent *propagating waves*. Imaginary wave numbers represent *attenuating* (*evanescent*) *waves* with an exponential (spatial) decay. The characteristic attenuation length (depth of penetration) is inversely proportional to the imaginary part of the wave number. The distance at which only 1% of the original amplitude remains is given from (4) by

$$l_{0.01} = \frac{|\ln(0.01)|}{|\mathrm{Im}\{\xi\}|}. \tag{12}$$

Except for a small frequency range, the smallest $|\mathrm{Im}\{\xi\}|$, termed *attenuation constant*, has a non-dimensional value of approximately 2, making the decay distance $l_{0.01}$ to be of the order of $2h$. At particularly small frequency regions, just below cut-off frequency (frequency at which $\xi = 0$), extremely small $\mathrm{Im}\{\xi\}$ is possible (Karp and Durban, 2005). Graphical representation of the possible modes in lower frequency region, as exposed by the relations (10) and (11), are plotted jointly on frequency map in Fig. B.1 in Appendix B for Poisson's ratio 1/3.

Due to the discrete nature of the solution in (8) and (9), the general solution (4) then consists of the sum of all possible modes and can be written in the form

$$u_x = \left[\sum_m \left(B_m U^m_{xd}(y) e^{i(\xi_m x-\omega t)}\right) + \sum_n \left(C_n U^n_{xe}(y) e^{i(\xi_n x-\omega t)}\right)\right]\left(\frac{\pi}{2h}\right),$$
$$u_y = \left[\sum_m \left(B_m U^m_{yd}(y) e^{i(\xi_m x-\omega t)}\right) + \sum_n \left(C_n U^n_{ye}(y) e^{i(\xi_n x-\omega t)}\right)\right]\left(\frac{\pi}{2h}\right), \tag{13}$$

where the four U functions are y dependent, describing the form of the wave mode, given explicitly in (A.11) in a non-dimensional form and B_m, C_n are the coefficients (amplitudes) of each mode to be determined in the next section.

It is of interest here to partition the response within the strip into near and far fields. The alternative expression for displacements in (13) is now given by

$$\boldsymbol{u}(x,y,t) = \sum_{n=1}^{N} A_n \boldsymbol{U}_n(y) e^{i(\xi_n x-\omega t)} + \sum_{n=N+1}^{\infty} A_n \boldsymbol{U}_n(y) e^{i\xi_n x} e^{-i\omega t}, \tag{14}$$

where the first summation is over the available N propagating waves making up the far-field response, and the second summation is over the evanescent waves, making up the near-field response. That formulation does not make a distinction between equivoluminal and dilatational modes, as in (13). Note the different meaning of the index n in (13) and in (14).

3. Amplitudes of the wave modes

The amplitudes of each mode in (13), B_m and C_n, are determined by the end data (1) at $x = 0$. The mathematical formalism for that determination for a mixed end data is worked out here based on the orthogonality and bi-orthogonality of the modes (the bi-orthogonality is due to Fraser, 1976).

Using the displacement and stress expressions given in (A.11) and (A.13) the general form of boundary excitation (1) can be written in the form

$$\sigma^0_x = \mu\left[\sum_m B_m S^m_{xd}(y) + \sum_n C_n S^n_{xe}(y)\right] e^{i(\xi_n x-\omega t)} = A_0 \mu \mathbb{S}(y) e^{-i\omega t},$$
$$u^0_y = \sum_m \left(B_m U^m_{yd}(y) e^{i(\xi_m x-\omega t)}\right) + \sum_n \left(C_n U^n_{ye}(y) e^{i(\xi_n x-\omega t)}\right) = 0, \quad \text{on } x = 0. \tag{15}$$

Completeness of the series expansion (13) is recalled here (e.g., Budreck and Rose, 1991) for justification of (15) for any excitation form to be prescribed over the end. Factoring out the time exponent and substituting $x = 0$ in (15) yields

$$\sum_m B_m S^m_{xd}(y) + \sum_n C_n S^n_{xe}(y) = A_0 \mathbb{S}(y),$$
$$\sum_m B_m U^m_{yd}(y) + \sum_n C_n U^n_{ye}(y) = 0. \tag{16}$$

Now, multiplication of the first of (16) by U^l_{xd} and the second by T^l_{xyd} (where l stands for lth mode) and integration over the strip width gives

$$\int_{-h}^{h}\left(\sum_m B_m S^m_{xd} U^l_{xd}\right)dy + \int_{-h}^{h}\left(\sum_n C_n S^n_{xe} U^l_{xd}\right)dy = A_0 \int_{-h}^{h}\left(\mathbb{S}(y) U^l_{xd}\right)dy,$$
$$\int_{-h}^{h}\left(\sum_m B_m U^m_{yd} T^l_{xyd}\right)dy + \int_{-h}^{h}\left(\sum_n C_n U^n_{ye} T^l_{xyd}\right)dy = 0. \tag{17}$$

Next we subtract the first of (17) from the second and interchange the order of integral and summation operators leading to

$$\left[\sum_m \int_{-h}^{h}\left(B_m U^m_{yd} T^l_{xyd}\right)dy - \sum_m \int_{-h}^{h}\left(B_m S^m_{xd} U^l_{xd}\right)dy\right] + \left[\sum_n \int_{-h}^{h}\left(C_n U^n_{ye} T^l_{xyd}\right)dy - \sum_n \int_{-h}^{h}\left(C_n S^n_{xe} U^l_{xd}\right)dy\right] = -A_0 \int_{-h}^{h}\left(\mathbb{S}(y) U^l_{xd}\right)dy. \tag{18}$$

The left hand of the equality consists of two contributions, namely, summation over m for dilatational waves with amplitude B_m and summation over n for distortional waves with amplitude C_n.

Two considerations lead to conclusion that the term associated with summation over n in (18) equals zero. Substitution of (A.11) and (A.14) leads to an explicit form of the integrands in these expressions to be given by

$$U^n_{ye} T^l_{xyd} = -2k_l k_n l \sin\left(\frac{\pi}{2} l \frac{y}{h}\right) \sin\left(\frac{\pi}{2} n \frac{y}{h}\right),$$
$$S^n_{xe} U^l_{xd} = -2k_l k_n n \cos\left(\frac{\pi}{2} l \frac{y}{h}\right) \cos\left(\frac{\pi}{2} n \frac{y}{h}\right). \tag{19}$$

Due to orthogonality of Fourier series, the integrals of these two terms (19) are zero for any $l \neq n$. For $l = n$ the integrals of these two terms are identical. Therefore, Eq. (18) takes the form

$$\sum_m \int_{-h}^{h}\left(B_m U^m_{yd} T^l_{xyd}\right)dy - \sum_m \int_{-h}^{h}\left(B_m S^m_{xd} U^l_{xd}\right)dy = -A_0 \int_{-h}^{h}\left(\mathbb{S}(y) U^l_{xd}\right)dy \tag{20}$$

and reordering will lead to

$$\sum_m B_m \int_{-h}^{h}\left(T^l_{xyd} U^m_{yd} - S^m_{xd} U^l_{xd}\right)dy = -A_0 \int_{-h}^{h}\left(\mathbb{S}(y) U^l_{xd}\right)dy. \tag{21}$$

The bi-orthogonality of the eigenstates, which is a derivative of the *elastic reciprocal theorem* (Gregory and Gladwell, 1983; Fraser, 1976), states that

$$\int_S \left(\tau^n_{xz} W^m - \sigma^m_x U^n\right)dS = 0, \quad m \neq n. \tag{22}$$

Therefore, the only terms to be retained on the left side of (21) are those with $m = l$ allowing for omission of the summation over m

$$B_m \int_{-h}^{h}\left(T^m_{xyd} U^m_{yd} - S^m_{xd} U^m_{xd}\right)dy = -A_0 \int_{-h}^{h}\left(\mathbb{S}(y) U^m_{xd}\right)dy. \tag{23}$$

From (23) the generally complex coefficient B_m can be deduced directly to yield

$$\frac{B_m}{A_0} = -\frac{1}{J_m}\int_{-h}^{h}\left(\mathbb{S}(y) U^m_{xd}\right)dy, \tag{24}$$

where

$$J_m = \int_{-h}^{h}\left(T^m_{xyd} U^m_{yd} - S^m_{xd} U^m_{xd}\right)dy. \tag{25}$$

Here J_m and U^m_{xd} are both properties of the wave modes and $\mathbb{S}(y)$ is the prescribed function over the end $x = 0$ in (1). All variables are complex in general to take an appropriate account for the phase of each mode.

The amplitudes of the equivoluminal modes C_n are found by the same procedure except for multiplication of (16) by the equivoluminal eigenfunctions U^l_{xe}, T^l_{xye} which lead to

$$\frac{C_n}{A_0} = -\frac{1}{J_n}\int_{-h}^{h}\left(\mathbb{S}(y) U^n_{xe}\right)dy \tag{26}$$

with

$$J_n = \int_{-h}^{h}\left(T^n_{xye} U^n_{ye} - S^n_{xe} U^n_{xe}\right)dy. \tag{27}$$

Expressions (24) and (26) provide the required relation between the excitation form $\mathbb{S}(y)$ (with amplitude A_0) and amplitude of each mode in (13).

The non-dimensional formulation (A.13) enables one to reduce the above formulas to simple expressions

$$J_m = ik_m\Omega^2\begin{cases}\cdot 2h, & \text{for } m=0,\\ \cdot h, & \text{for } m=2,4,6,\end{cases} \tag{28}$$

$$J_n = -ik_n\Omega^2 h, \quad \text{for } n=2,4,6,\ldots, \tag{29}$$

which lead to coefficients to be written as

$$\frac{B_0}{A_0} = -\frac{1}{\Omega^2 2h}\int_{-h}^{h}(\mathbb{S}(y))dy, \tag{30a}$$

$$\frac{B_m}{A_0} = -\frac{1}{\Omega^2 h}I_m, \quad m=2,4,6,\ldots, \tag{30b}$$

$$\frac{C_n}{A_0} = -\frac{in}{k_n}\frac{1}{\Omega^2 h}I_n, \quad n=2,4,6,\ldots, \tag{31}$$

where

$$I_m \equiv \int_{-h}^{h}\left(\mathbb{S}(y)\cos\left(\frac{\pi}{2}m\frac{y}{h}\right)\right)dy, \quad I_n \equiv \int_{-h}^{h}\left(\mathbb{S}(y)\cos\left(\frac{\pi}{2}n\frac{y}{h}\right)\right)dy. \tag{32}$$

From here, one obtains that $I_m = I_n$ for $m = n$.

It turns out that since the cross-sectional form of the various modes are either sine or cosine functions, the amplitudes of each mode are determined explicitly by a standard Fourier analysis (30)–(31).

Let us consider the resulting surface axial strain as representing the response of the strip. Using relations (30–31) in (A.12) will yield simple expressions for the axial surface strain. Surface strain associated with the fundamental mode take the form

$$\left.\frac{\varepsilon_x(x,t)}{A_0}\right|_{y=h} = \frac{1}{\kappa^2}\frac{1}{2h}\int_{-h}^{h}\mathbb{S}(y)dy\left[e^{i\frac{\pi}{2}\left(k_0\frac{x}{h}-\Omega\frac{t}{t_c}\right)}\right], \quad m=0, \tag{33}$$

while the contribution of the higher modes is given by

$$\left.\frac{\varepsilon_x(x,t)}{A_0}\right|_{y=h} = \sum_{m=2}^{\infty}\left(\frac{k_m}{\Omega}\right)^2\frac{(-1)^{\frac{m}{2}}}{h}I_m e^{i\frac{\pi}{2}\left(k_m\frac{x}{h}-\Omega\frac{t}{t_c}\right)} + \sum_{n=2}^{\infty}\left(\frac{n}{\Omega}\right)^2\frac{(-1)^{\frac{n}{2}}}{h}I_n e^{i\frac{\pi}{2}\left(k_n\frac{x}{h}-\Omega\frac{t}{t_c}\right)}. \tag{34}$$

Here, k_0 is a real valued wave number of the fundamental mode given explicitly by $k_0 = \Omega/\kappa$ with t_c defined by $t_c = 2h/C_T$.

In a non-dissipative media (as assumed here) the propagating waves do not attenuate down the strip and have an average power communication (per unit length in the z direction, average over strip width $2h$, and average over time period $T = 2\pi/\omega$) given by

$$\langle P\rangle \equiv \frac{1}{T}\frac{1}{2h}\int_0^T\int_{-h}^{h}(\boldsymbol{\sigma}\cdot\dot{\boldsymbol{u}})dydt. \tag{35}$$

That expression is valid at any cross-section of the strip irrespective of the existence of evanescent waves. For harmonic waves, Eq. (35) will take the form

$$\langle P_j\rangle = -\frac{1}{4h}\omega\mu|A_j|^2\mathrm{Im}\{J_j\}, \tag{36}$$

for any wave mode j with amplitude A_j, where J_j is either J_m defined in (25) or J_n given in (27). Since evanescent waves are characterized by imaginary wave numbers, from (28) and (29) it can be confirmed that $\mathrm{Im}\{J_j\} = 0$, indicating that the total net power communicated by evanescent waves is indeed zero. Using the non-dimensional formulation, the average energy transfer rate (36) becomes

$$\left\langle P_d^0\right\rangle = -\frac{\mu}{8h^2}\frac{C_T}{\kappa}A_0^2 I_0^2 m = 0, \tag{37a}$$

$$\left\langle P_d^m\right\rangle = -\frac{\mu}{4h^2}C_T\frac{k_m}{\Omega}A_0^2 I_m^2 m = 2,4,6,\ldots,M, \tag{37b}$$

for the dilatational propagating modes and

$$\left\langle P_e^n\right\rangle = -\frac{\mu}{4h^2}C_T\frac{n}{\Omega}A_0^2 I_n^2, \quad n=2,4,6,\ldots,N, \tag{38}$$

for the distortional propagating modes. It should be kept in mind that the number of available propagating modes, M and N, depends on the frequency, as shown in Fig. B.1.

4. Simple excitations

To illustrate the method for coefficient determination and the nature of dynamic end-effects, let us examine the exact response of a strip to three well-defined excitations, designated by $\mathbb{S}_a$, $\mathbb{S}_b$, and $\mathbb{S}_c$. The excitations are harmonic in time with a frequency taken as a controlled parameter. Poisson's ratio $\nu = 1/3$ is assumed, whenever required.

4.1. Uniform excitation

Uniform excitation is given by (1) with

$$\mathbb{S}_a(y) = 1. \tag{39}$$

The only non-zero integral in (32) is

$$I_m = \int_{-h}^{h}\left(\mathbb{S}_a\cos\left(\frac{\pi}{2}m\frac{y}{h}\right)\right)dy = 2h, \tag{40}$$

for $m = 0$. Then, by (30a) we find that the non-zero coefficient B_0 is given by

$$\frac{B_0}{A_0} = -\frac{1}{\Omega^2}. \tag{41}$$

From here, it follows that excitation (39) can excite only the fundamental mode regardless of the frequency with which it oscillates. The expression for the surface strain in (33) will become

$$\left.\frac{\varepsilon_x(x,t)}{A_0}\right|_{y=h} = \frac{1}{\kappa^2}e^{i\frac{\pi}{2}\left(k_0\frac{x}{h}-\Omega\frac{t}{t_c}\right)}, \tag{42}$$

representing harmonic wave with an amplitude coinciding with the one-dimensional solution given by

$$\sigma_x = (\lambda+2\mu)\varepsilon_x \Rightarrow \varepsilon_x = \frac{1}{\kappa^2}\frac{\sigma_x}{\mu}. \tag{43}$$

That excitation can be considered as an analogue of strength of material theory according to which the end load has an identical form to the inner solution, and therefore, the end-effects are actually absent.

By (40) and (37a), energy influx of the propagating mode is given by

$$\left\langle P_d^0\right\rangle = -\frac{\mu}{2}\frac{C_T}{\kappa}A_0^2. \tag{44}$$

4.2. Cosine excitation

Cosine excitation is defined by

$$\mathbb{S}_b(y) = \cos\left(\pi\frac{y}{h}\right) \tag{45}$$

and from (32) one obtains that the only non-zero term is $I_2 = h$ for $m = n = 2$. The corresponding coefficients (30) and (31) are B_2 and C_2 given by

$$\frac{B_2}{A_0} = -\frac{1}{\Omega^2}, \tag{46}$$

$$\frac{C_2}{A_0} = -\frac{2i}{\Omega^2\sqrt{\Omega^2-4}}. \tag{47}$$

Inserting (46) and (47) in (34) yield simple expression for the surface strain

$$\left.\frac{\varepsilon_x(x,t)}{A_0}\right|_{y=h} = \left(\frac{4}{\Omega^2}-1\right)e^{i\frac{\pi}{2}\left(k_m\frac{x}{h}-\Omega\frac{t}{t_c}\right)} - \frac{4}{\Omega^2}e^{i\frac{\pi}{2}\left(k_n\frac{x}{h}-\Omega\frac{t}{t_c}\right)}, \quad m=n=2. \tag{48}$$

Three qualitatively different frequency regions can be identified according to the nature of the wave numbers k_m and k_n in (10) and (11) for $m = n = 2$:

(1) $\Omega < 2$ – below the first distortional cut-off frequency. From (10) and (11), both wave numbers are purely imaginary. Designating the wavenumbers by $k_m = ik_m^*$ and $k_n = ik_n^*$, the axial behavior of surface strain (48) will take the form

$$\left.\frac{\varepsilon_x(x)}{A_0}\right|_{y=h} = \left(\frac{4}{\Omega^2}-1\right)e^{-\frac{\pi}{2}k_m^*\frac{x}{h}} - \frac{4}{\Omega^2}e^{-\frac{\pi}{2}k_n^*\frac{x}{h}}. \tag{49}$$

That response is completely confined to the end of the strip and comprises an end effect (edge vibration). Then, by (36), no energy influx is possible regardless of the amplitude of the excitation A_0.

(2) $2 < \Omega < \kappa^2$ – between the first dilatational and the first distortional cut-off frequencies. The distortional wavenumber is real and dilatational is purely imaginary (see Fig. B.1).

(3) $\kappa^2 < \Omega$ – above both cut-off frequencies. Both wave numbers are purely real. Under these conditions, the complete response of the strip is a superposition of the two propagating modes given in (48). None of the evanescent waves are excited rendering no end effect at all.

4.3. Half-cosine excitation

Half-cosine excitation is defined here by

$$\mathbb{S}_c(y) = \cos\left(\frac{\pi}{2}\frac{y}{h}\right), \tag{50}$$

the integration of which in (32) gives

$$I_m = \frac{4h\cos\left(m\frac{\pi}{2}\right)}{\pi(1-m^2)}, \tag{51}$$

for any m and n. From (51) we find that no mode can be said to remain unexcited. Let us again focus on the axial strain at the surface $y = h$. For the fundamental mode, $m = 0$, (51) leads to

$$\left.\frac{\varepsilon_{xd}^0(x,t)}{A_0}\right|_{y=h} = \frac{1}{\kappa^2}\frac{2}{\pi}e^{i\frac{\pi}{2}\left(k_n\frac{x}{h}-\Omega\frac{t}{t_c}\right)}, \quad m=0. \tag{52}$$

Insertion of (51) into (34) yields surface strains associated with the dilatational modes

$$\left.\frac{\varepsilon_{xd}^m(x,t)}{A_0}\right|_{y=h} = \left[\frac{4}{\pi}\left(\frac{k_m}{\Omega}\right)^2\frac{1}{1-m^2}\right]e^{i\frac{\pi}{2}\left(k_m\frac{x}{h}-\Omega\frac{t}{t_c}\right)}, \quad m=2,4,6,\ldots \tag{53}$$

and for the equivoluminal modes

$$\left.\frac{\varepsilon_{xe}^n(x,t)}{A_0}\right|_{y=h} = \left[\frac{4}{\pi}\left(\frac{n}{\Omega}\right)^2\frac{1}{1-n^2}\right]e^{i\frac{\pi}{2}\left(k_n\frac{x}{h}-\Omega\frac{t}{t_c}\right)}, \quad n=2,4,6,\ldots. \tag{54}$$

The contribution of each mode, and particularly of the evanescent modes, is emphasized here. In the frequency region below the first cut off, $\Omega < 2$, from (10) and (11) one finds that only one propagating mode is available, given in (52). All evanescent waves, (53) and (54), attenuate with a typical distance given by (12). The higher the mode, the more localized its effect. The axial attenuation of the twelve first evanescent modes (6×2), for $\Omega = 0.5$, is traced in Fig. 1. It can be observed that the first attenuating mode, $m = n = 2$, can be regarded as a bound on attenuation distance, as frequently estimated from Eq. (12). The complete sum of these modes is shown in Fig. 2.

It is convenient to illustrate the contribution of the evanescent waves to the complete dynamic response of the strip by comparing the amplitude of the response at any distance x from the end to the amplitude of the sole propagating mode. That ratio of the total dynamic response to the far field response (the amplitude of the propagating wave) can be based on various field parameters. For the purpose of the present work, it is suitable to use the axial surface strain as typical, rendering the ratio to be defined by

$$SVR_\varepsilon(x) = \frac{\varepsilon_{x,total}(x)}{\varepsilon_{x,far\ field}} = \frac{\varepsilon_{x,propagating} + \varepsilon_{x,evanescent}}{\varepsilon_{x,propagating}} \tag{55}$$

and can be regarded as a deviation of the near field from the far field. As such, it is termed Saint-Venant ratio (SVR) with a subscript ε designating the ratio evaluated in terms of surface strain. Since the evanescent waves die out at some distance $l_{0.01}$, approximated by (12), SVR (x) has an asymptote at SVR = 1. For the particular solution derived above in (52)–(54), for a frequency range $\Omega < 2$ with only one propagating mode $m = 0$, SVR (55) will take the form

$$SVR_\varepsilon(x) = \frac{\varepsilon_{xd}^0 + \sum_{m=2}^{\infty}\varepsilon_{xd}^m + \sum_{n=2}^{\infty}\varepsilon_{xe}^n}{\varepsilon_{xd}^0}, \quad m,n=2,4,6,\ldots. \tag{56}$$

For practical purposes, the infinite series will be truncated here at $m = n = 12$ leading to a finite sum of the evanescent modes, given by

$$SVR_\varepsilon(x) = \frac{\varepsilon_{xd}^0 + \sum_{m=2}^{12}\varepsilon_{xd}^m + \sum_{n=2}^{12}\varepsilon_{xe}^n}{\varepsilon_{xd}^0}. \tag{57}$$

That ratio, along with the amplitude of the propagating wave and the sum of the evanescent waves, for excitation frequency $\Omega = 0.5$, is traced in Fig. 2. It is noted that time dependence of the strain field is omitted in the definition of SVR.

To estimate the sufficiency of first 13 modes for accurate description of the axial behavior of the strip in general, and SVR in particular, the deviation of the stress associated with these modes from the actual boundary data (50) is examined. That deviation is defined by

$$\Delta\sigma|_{x=0} = \mathbb{S}_c(y) - \sigma(y)|_{x=0} \tag{58}$$

with

$$\sigma(y)|_{x=0} = \sum_{m=0}^{12}B_m S_{xd}^m + \sum_{n=2}^{12}C_n S_{xe}^n. \tag{59}$$

The deviation (58) is evaluated for the first 11 modes (1 propagating and 5×2 evanescent) and first 13 modes ($1 + 6 \times 2$) and traced in Fig. 3 for the same frequency $\Omega = 0.5$. The largest deviation is at the surface with magnitude of about 4%. From Fig. 1 and from Eq. (12) it is evident that deviation is nullified at distances beyond $x = h/10$. Additional modes with m, $n > 12$, will further decrease the deviation, which might be significant only for $x/h < 0.1$.

5. Variation on reference excitation

The general formulation for calculation of the amplitude of each mode traced in Section 3 is used here to derive dynamic responses of a strip subjected to end excitations with various irregularities. These will be compared to strip response subjected to an uniform excitation, $\mathbb{S}_a$, worked out in Section 4.1.

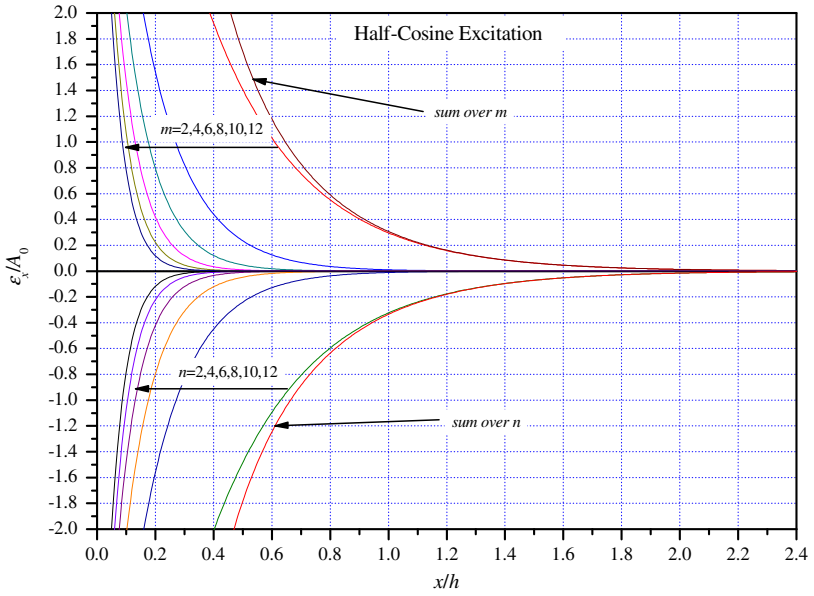

Fig. 1. Surface axial strain for the first 12 modes calculated from (53) and (54), for a half-cosine excitation (50). The sums of the dilatational (m) and the distortional (n) modes are shown by separate curves.

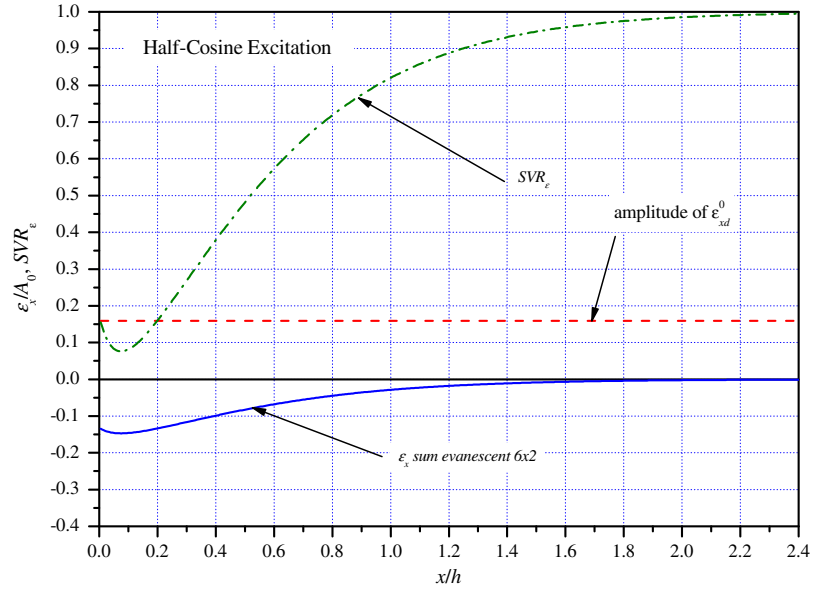

Fig. 2. Surface axial strain for first fundamental mode (maximum amplitude), the sum of the evanescent modes shown in Fig. 1, and SVR for a half-cosine excitation (50).

As a simple example for excitations slightly deviating from an uniform distribution, let us consider two basic cases (both symmetric): non-uniformity at the centerline $y = 0$ of the strip and non-uniformity at the edges $y = \pm h$. The first case can be written in a parametric form by

$$\mathbb{S}_{in}(y) = 1 - dH(y + wh) + dH(y - wh), \tag{60}$$

where H is the *Heaviside Unit* step function, d and w stand for the depth and the width of the non-uniformity, respectively. This non-uniformity represents a reduced stress at the center of the edge. The reduction level is dictated by d with partial reduction if $d < 1$ and complete reduction if $d = 1$. The width of the reduced stress area is defined by w. The outer edge non-uniformity is defined by

$$\mathbb{S}_{out}(y) = (1 - d)H(y + h) + dH(y + (1 - w)h) - dH(y - (1 - w)h) - (1 - d)H(y - h) \tag{61}$$

with the same meaning of the parameters d and w as in (60). The particular values for the non-uniformities evaluated here, and the designation of each form, are given in Table 1. The general expression for the integral I_m, defined by (32), is given in Table 1 for excitation (60).

For the purpose of the present work, only surface axial strains are evaluated explicitly, given by (33) for the first fundamental mode $m = 0$ and by (34) for the higher modes. The effect of various forms of excitation on the response of the strip is analyzed based on the Saint Venant Ratio, defined in (55) and evaluated numerically for $\Omega = 0.5$ with a finite number of modes as given by (57). The result is shown in Fig. 4 suggesting that even small deviation

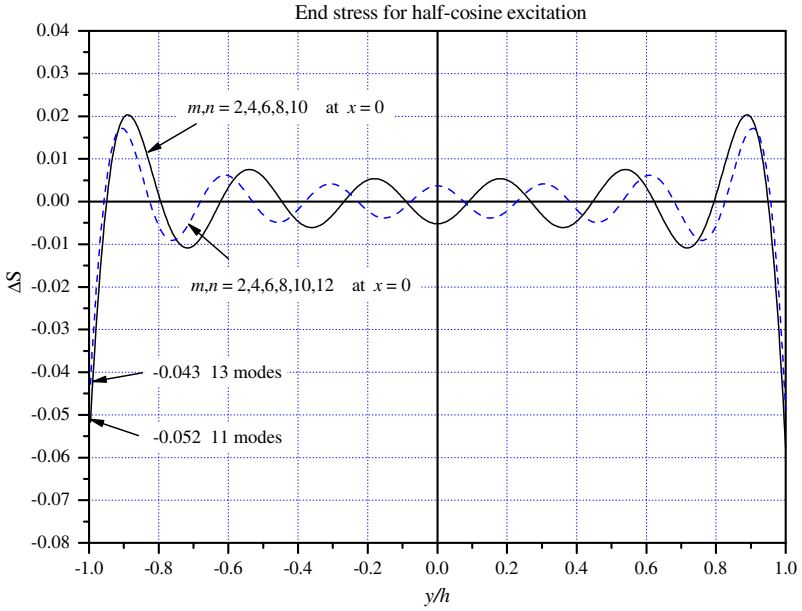

Fig. 3. The difference between the applied excitation form (50) and the traction associated with first 11 modes up to $m = n = 10$ and for first 13 modes up to $m = n = 12$.

Table 1
The particular values for the non-uniformity in (60) and (61). Also shown are the theoretical and the numerical values for the SVR at $x = 0$.

Form	d	w	SVR ($x = 0$) *theoretical*	SVR ($x = 0$) *numerical*	$I_m(m \neq 0)$
$\mathbb{S}_{1\text{-in}}$	1	0.1	1.11	1.049	$-\frac{4d}{\pi m}\sin\left(w\frac{\pi}{2}m\right)$
$\mathbb{S}_{2\text{-in}}$	1	0.2	1.25	1.29	
$\mathbb{S}_{3\text{-in}}$	1	0.3	1.43	1.431	
$\mathbb{S}_{4\text{-in}}$	0.5	0.2	1.11	1.12	
$\mathbb{S}_{5-out}$	1	0.1			

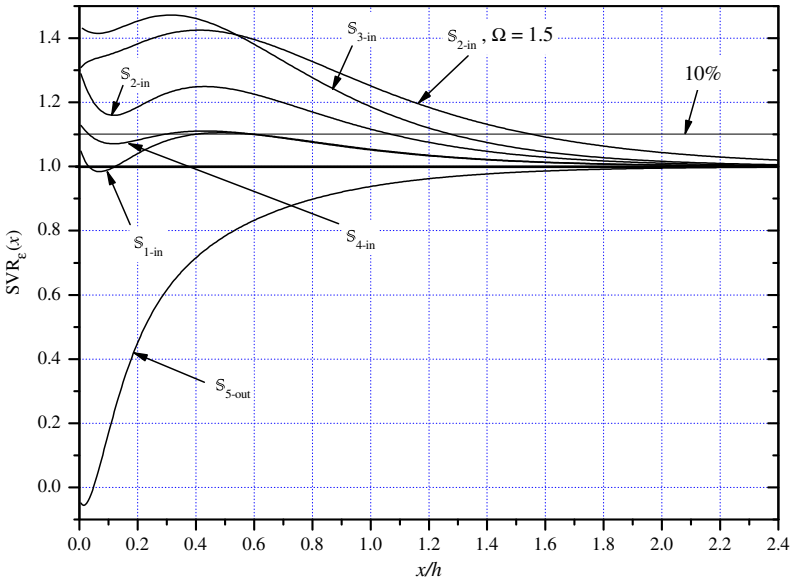

Fig. 4. SVR based on surface axial strain (57) for five excitations given in Table 1 with frequency $\Omega = 0.5$ and $\mathbb{S}_{2\text{-in}}$ excitation also with frequency $\Omega = 1.5$. The horizontal line designated by 10% represents deviation from SVR = 1 for an ideal uniform excitation (39).

from the uniform excitation $\mathbb{S}_{1\text{-in}}$ generates 10% difference in SVR at a distance of $x \approx h/2$.

As a rough estimation for a possible error in truncation of the complete series solution at $m = n = 12$ the theoretical SVR at $x = 0$ is compared to the numerical result. For the simple excitation form given by (60), the theoretical SVR at $x = 0$ is given by

$$SVR_\varepsilon(x = 0) = \frac{h - wd}{h}, \tag{62}$$

reflecting the ratio of the effective contact area at $x = 0$ to the actual cross-section area of the strip far from the excited end. The values of that theoretical SVR and its numerical calculation for the four excitations defined by (60) are given in Table 1. The largest deviation is for $\mathbb{S}_{1\text{-in}}$, which, according to decay distances of higher modes, is confined to a distance not exceeding $x = h/10$.

Based on the estimation of sufficiency of 13 modes suggested above in Fig. 3, it is expected that the inaccuracy of the SVR curves in Fig. 4 is limited to $x/h < 0.1$.

To appreciate the effect of frequency on detectability of changes in the form of the excitation, SVR for excitation $\mathbb{S}_{2\text{-in}}$ with $\Omega = 1.5$ is shown in Fig. 4 as well. It is apparent that the affected zone is larger in comparison to the same excitation form with $\Omega = 0.5$. This can be inferred directly from the frequency map in Fig. B.1 showing a reduced attenuation constant at higher frequencies.

6. Discussion

To begin with, let us examine the results of Section 4 with reference to the question of dynamic equivalence of loads. In particular, it is questioned whether it is possible to generate an identical far-field response in a strip by differently distributed loads. According to (14), beyond the largest distance $l_{0.01}$ (defined by (12) with the smallest $|\mathrm{Im}\{\xi\}|$), only propagating waves constitute the displacement field. That field is determined uniquely by ω, ξ_n (defining $\boldsymbol{U}_n$ through (A.11)), and A_n (which is actually B_n and C_n in the non-dimensional formulation in (A.11)). In the frequency range $\Omega < 2$, only the fundamental mode can be excited with the wave number given by $k_0 = \Omega/\kappa$. From (30a), the amplitude of that mode is

$$B_0 = -\frac{A_0}{\Omega^2 2h}\int_{-h}^{h}\mathbb{S}dy. \tag{63}$$

Therefore, in order to obtain an identical far field response, B_0, by two differently distributed loads, $\mathbb{S}_i$ and $\mathbb{S}_j$, having an identical frequency; their amplitude, A_{0i} and A_{0j}, should be adjusted according to the equality

$$A_{0i}\int_{-h}^{h}\mathbb{S}_i dy = A_{0j}\int_{-h}^{h}\mathbb{S}_j dy. \tag{64}$$

Such an adjustment will also result in an identical power, according to (37a).

As a particular example, consider the uniform $\mathbb{S}_a$ and the half-cosine $\mathbb{S}_c$ excitations with amplitudes A_{0a} and A_{0c}, respectively. By relation (64), with the aid of (40) and (51), these excitations will be equivalent if their amplitudes are related by

$$A_{0a} = A_{0c}\frac{2}{\pi}. \tag{65}$$

This leads to the following conclusion: both excitations, $\mathbb{S}_a$ and $\mathbb{S}_c$, with amplitudes related by (65), will generate identical far-field response (ω, ξ_n, and B_0) and will be undistinguishable if judged upon the far field alone. These loads are termed *dynamically equivalent*, and as such, illustrate the interpretation and the validity of DSVP suggested by Karp (2009). According to that interpretation, two dynamically equivalent loads will generate identical strain filed far from the loaded area. That interpretation is not a simple extension of the classical SVP since in the static case the equivalence is judged upon static equivalents, while here, the equivalence is judged upon average power (intensity) of the excitation. Nevertheless, it was shown that both interpretations coincide in the limit of vanishing frequency (Karp, 2009).

Since the dynamic response of the whole strip can not be identical for differently distributed loads, let us seek the differences in response of the strip subjected to any dynamically equivalent loads. The difference in response will be confined to the vicinity of the excited edge, as dictated by the evanescent waves (the second summation in (14)). In the particular example of uniform excitation, $\mathbb{S}_a$, discussed above, none of the evanescent waves is excited, which by (55) results in SVR = 1 for any x. For $\mathbb{S}_c$, on the other hand, SVR is x dependent as shown in Fig. 2. That sensitivity of the SVR to the form of the excitation is the key for the health monitoring of joints.

It is interesting to note that $\mathbb{S}_a$ and $\mathbb{S}_b$ can not be made dynamically equivalent by amplitude adjustment (64) since they generate different propagating modes at any frequency (different k's for identical Ω). Moreover, excitation $\mathbb{S}_b$ is incapable of inducing continuous influx of energy at frequencies below the first cut-off. It is not expected that such situation can arise in a waveguide with free surfaces (e.g., Karp and Durban, 2005).

This point emphasizes the substantial difference between orthogonality and bi-orthogonality properties of the wave modes. The mathematical relations between the modes can be interpreted in the following way. From (19) one finds that distortional modes are orthogonal to dilatational modes for $m \neq n$ and bi-orthogonal for $m = n$. From (22) the dilatational modes are bi-orthogonal to other dilatational modes. The same holds for distortional modes. The physical meaning of orthogonality is that, on average over the cross-section, stresses of distortional modes do zero net work over the displacements of the dilatational modes, and vise versa. On the other hand, bi-orthogonality means that the average work of shear stresses of one mode over the displacements of the other mode is equal and opposite in sign to the average work of the normal stresses of the other mode over the displacements of the first mode. Since the dilatational and distortional modes are coupled in a strip with free surfaces, no orthogonality exists.

Finally, let us discuss the results as they might be related to monitoring the health of structural joints. The particular question can be stated as follows: is it possible, by monitoring the dynamical response of a plate, to identify incipient changes at its joint?.

Eq. (64) exposes dynamic equivalence, according to which various forms of excitation can produce identical far field response (see Karp, 2009 for analogous derivation for a strip with free surfaces). Therefore, relying on measurements within the far field alone will not expose different forms of excitations. By the same token, measurement within the near-field alone can not lead to univocal conclusion on changes of the form of the excitation since the change in strain within the near-field can be also attributed to change in intensity of the excitation.

In search for a reliable signature of the form of an excitation, one finds that the SVR does fulfill that requirement. The definition of SVR (x) in (55) along with the associated wave mode formulation discloses that SVR is a sort of convolution of wave guide property encompassed in k and the form of the excitation $\mathbb{S}$. Therefore, if the properties of the waveguide remain unchanged (no change in k_n), SVR can be considered as a *signature* of the *form* of the excitation alone. Hence, it can be stressed that a combination of measurements in the far- and the near-fields (a point wise tracing of SVR (x)) can provide the required data for inferring on a *change* in the form of the excitation. In such combination, the far-field measurement is used to scale the near-field measurement, screening out changes originated from a change in amplitude of the excitation. From Fig. 4 it can be deduced that measurement of surface strain within the region $0.4 < x/h < 1.2$ using a gauge with minimal reading detection of 10% (a modest requirement), will enable easy detection of small changes in the form of the excitation, such as $\mathbb{S}_{1\text{-in}}$ and $\mathbb{S}_{5\text{-out}}$.

Relevance of the results obtained above to actual problems where SHM is sought can be supported by the following observations. Qualitative and quantitative characteristics of the dynamic response of a strip with sliding surfaces (Fig. B.1) are typical to

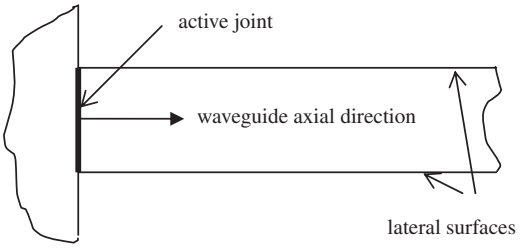

Fig. 5. Schematic view of a joint between a beam-like structure (waveguide) and a main frame.

other waveguides with different conditions on the surfaces, as inferred from the similarity of various frequency maps (e.g., Mindlin, 1960). An end of a waveguide can be viewed as a joint to which an external excitation is applied (Fig. 5). Alternatively, that end can be a reflecting end if a wave is propagated from within the waveguide. Healthy joint, regardless of the exact actual from of the connection, is characterized by particular SVR which can be traced experimentally at discrete distances x from the end. Even incipient alteration of the joint condition, as shown in Section 5, will alter the end data generating a new SVR signature. That analogy between variation of end conditions considered in Section 5 and actual damage to joint, though not very strict, can be adequate to demonstrate qualitatively, and even quantitatively, the potential of end effects as a structural marker for SHM. For example, any excitation in Table 1 can be considered as a reference excitation with other excitation as representing a damaged joint.

As a further support for the way the above results can be related to waveguides with free lateral faces, let us compare the results obtained here to previously reported experimental studies. Transient end effects in a cantilever beam were measured by Karp et al. (2008). In that work, end effects are the result of reflecting waves in a beam with free surfaces (passive joint). It was found that the far field response is completely not sensitive to small changes in a way the clamping of the beam was realized, while measurements within the near field exposed high sensitivity to such variations. The magnitude of the estimated near-field is similar to the obtained here in Fig. 4, and could be expected based on the similarity of the frequency maps for strips with various surface conditions (Mindlin, 1960).

Impact excitation of a rod at its end (active joint) with impactors having various contact surfaces is reported by Karp et al. (2009). It was found that the near field, within 1.4 diameters from the end, is sensitive to the form of the contact area with only rudimental sensitivity of the far-field. Finite element calculation of the response of a rod impinged by different strikers (Fig. 12 in Karp et al., 2009) exposed axial distribution of surface strain which is similar to the obtained here in Fig. 4. This similarity could also be expected based on the similarity of frequency maps of strip and rod waveguides (Graff, 1975, Figs. 8.9 and 8.17; Miklowitz, 1978, p. 222).

7. Concluding remarks

A simple case of an ideal waveguide, represented by an elastic, semi-infinite strip with sliding surfaces, was used to examine analytically the precise near-field sensitivity to variations in the form of end-excitation. The exact formulation of the relation between the form of the excitation and the amplitudes of each propagating and evanescent wave modes were calculated using orthogonality and bi-orthogonality of the modes. Several "ideal" and "deviating" excitations were worked out to illustrate the sensitivity of the surface strain to the form of the excitation. These excitations were regarded as idealization of healthy and damaged joints. The dynamic end effects, quantitatively defined by Saint-Venant Ratio, are shown to be an efficient structural marker of the joint condition. It turns out that by using that marker, incipient variation in end data conditions can be monitored with reasonably simple equipment.

The results obtained appear to be valid as a rough guide for design of SHM system for joints under more realistic conditions of strips with free surfaces and with end data not necessarily mixed. The mixed end data at $x = 0$ studied here was chosen to enable the use of bi-orthogonality relations. Non-mixed end data can be studied by using other methods, such as employed by Gregory and Gladwell (1983, 1989) or by Babenkova and Kaplunov (2005). In a subsequent work, similar treatment will be applied to a passive joint, where the excitation source is located in the far-field of the strip.

Appendix A. Symmetric wave modes derivation and non-dimensional formulation

The displacement field in a wave guide, assuming separation of variables, is written in the form

$$\boldsymbol{u}(x,y,t) = \boldsymbol{U}(y)e^{i(\xi x-\omega t)}. \tag{A.1}$$

Following Achenbach (1973), the displacement potential is given by

$$\varphi = f(y)e^{i(\xi x-\omega t)}, \quad \psi = g(y)e^{i(\xi x-\omega t)} \tag{A.2}$$

with

$$\begin{aligned} f(y) &= A\sin(\gamma y) + B\cos(\gamma y),\\ g(y) &= C\sin(\delta y) + D\cos(\delta y), \end{aligned} \tag{A.3}$$

where

$$\gamma^2 \equiv \frac{\omega^2}{C_L^2} - \xi^2, \quad \delta^2 \equiv \frac{\omega^2}{C_T^2} - \xi^2 \tag{A.4}$$

with C_L and C_T as the longitudinal and transversal phase velocities in an infinite medium, respectively. Here the coefficients A, B, C, D are complex amplitudes which allow for phase change for each mode. The displacement components are derived from (A.2) by

$$u_x = \frac{\partial\varphi}{\partial x} + \frac{\partial\psi}{\partial y}, \quad u_y = \frac{\partial\varphi}{\partial y} - \frac{\partial\psi}{\partial x}. \tag{A.5}$$

For symmetric fields $A = D = 0$. Then, equations (A.5) and (A.2) lead to the two displacement components

$$\begin{aligned} u_x &= (iB\xi\cos(\gamma y) + C\delta\cos(\delta y))e^{i(\xi x-\omega t)},\\ u_y &= (-B\gamma\sin(\gamma y) - iC\xi\sin(\delta y))e^{i(\xi x-\omega t)}. \end{aligned} \tag{A.6}$$

The strains follow from (A.6) as

$$\begin{aligned} \varepsilon_x &= \left(-B\xi^2\cos(\gamma y) + iC\xi\delta\cos(\delta y)\right)e^{i(\xi x-\omega t)},\\ \varepsilon_y &= \left(-B\gamma^2\cos(\gamma y) - iC\delta\xi\cos(\delta y)\right)e^{i(\xi x-\omega t)},\\ \varepsilon_{xy} &= \frac{1}{2}\left(-2iB\gamma\xi\sin(\gamma y) + C(\xi^2-\delta^2)\sin(\delta y)\right)e^{i(\xi x-\omega t)} \end{aligned} \tag{A.7}$$

and by Hook's law we obtain the stresses in the form

$$\begin{aligned} \sigma_x &= \mu\left[-B\left(\frac{\omega^2}{C_T^2} - 2\gamma^2\right)\cos(\gamma y) + C2i\delta\xi\cos(\delta y)\right]e^{i(\xi x-\omega t)},\\ \sigma_y &= \mu\left[-B\left(\frac{\nu}{1-\nu}\frac{\omega^2}{C_T^2} + 2\gamma^2\right)\cos(\gamma y) - C2i\delta\xi\cos(\delta y)\right]e^{i(\xi x-\omega t)},\\ \tau_{xy} &= \mu\left[-B2i\gamma\xi\sin(\gamma y) + C\left(\frac{\omega^2}{C_T^2} - 2\delta^2\right)\sin(\delta y)\right]e^{i(\xi x-\omega t)}, \end{aligned} \tag{A.8}$$

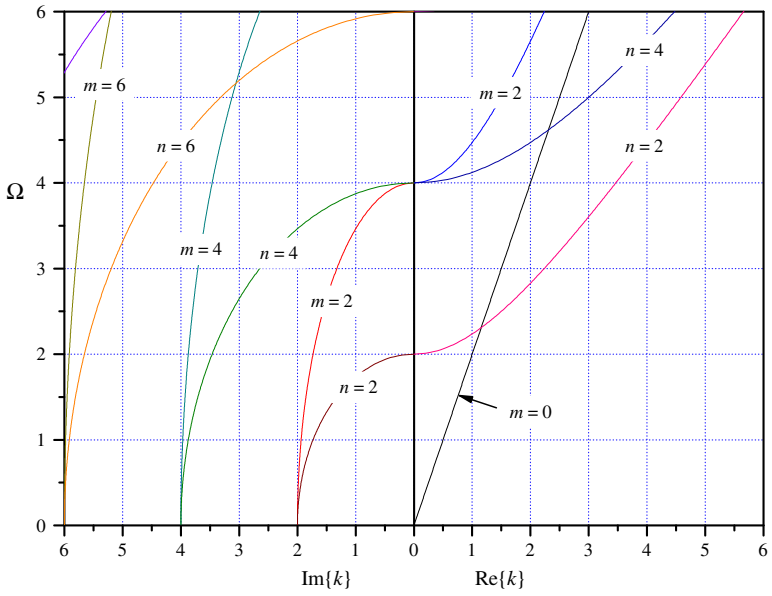

Fig. B.1. Attenuation map for lowest wave numbers for a plate with sliding surfaces calculated from Eqs. (10) and (11).

where μ and v are the shear modulus and Poisson's ratio, respectively. Introducing non-dimensional variables

$$k \equiv \frac{2h}{\pi}\xi, \quad \Omega \equiv \frac{2h}{\pi C_T}\omega, \quad \frac{1}{\kappa^2} = \left(\frac{C_T}{C_L}\right)^2 = \frac{1-2v}{2(1-v)} \tag{A.9}$$

and taking into account the discrete nature of the solution (8) and (9), the displacements derived above will take the form

$$\begin{aligned} u_x &= \left[\sum_{m=0}^{\infty} B_m U_{xd}^m(y) e^{i(\xi_m x-\omega t)} + \sum_{n=2}^{\infty} C_n U_{xe}^n(y) e^{i(\xi_n x-\omega t)}\right]\left(\frac{\pi}{2h}\right), \\ u_y &= \left[\sum_{m=0}^{\infty} B_m U_{yd}^m(y) e^{i(\xi_m x-\omega t)} + \sum_{n=2}^{\infty} C_n U_{ye}^n(y) e^{i(\xi_n x-\omega t)}\right]\left(\frac{\pi}{2h}\right) \end{aligned} \tag{A.10}$$

with the cross-sectional form defined by

$$\begin{aligned} U_{xd}^m(y) &\equiv ik_m \cos\left(\tfrac{\pi}{2} m \tfrac{y}{h}\right), \quad U_{xe}^n(y) \equiv n \cos\left(\tfrac{\pi}{2} n \tfrac{y}{h}\right), \\ U_{yd}^m(y) &\equiv -m \sin\left(\tfrac{\pi}{2} m \tfrac{y}{h}\right), \quad U_{ye}^n(y) \equiv -ik_n \sin\left(\tfrac{\pi}{2} n \tfrac{y}{h}\right), \end{aligned} \tag{A.11}$$

for any wave mode m and n. The axial strain is given by

$$\begin{aligned} \varepsilon_x = &\sum_{m=0}^{\infty} -B_m \left(\frac{\pi}{2h}\right)^2 k_m^2 \cos\left(\frac{\pi}{2} m \frac{y}{h}\right) e^{i\frac{\pi}{2}\left(k_m \frac{x}{h} - \Omega \frac{t}{t_c}\right)} \\ &+ \sum_{n=2}^{\infty} iC_n \left(\frac{\pi}{2h}\right)^2 k_n n \cos\left(\frac{\pi}{2} n \frac{y}{h}\right) e^{i\frac{\pi}{2}\left(k_n \frac{x}{h} - \Omega \frac{t}{t_c}\right)} \end{aligned} \tag{A.12}$$

and stresses are

$$\begin{aligned} \sigma_x &= \mu\left[\sum_{m=0}^{\infty} B_m S_{xd}^m(y) e^{i(\xi_m x-\omega t)} + \sum_{n=2}^{\infty} C_n S_{xe}^n(y) e^{i(\xi_n x-\omega t)}\right]\left(\frac{\pi}{2h}\right)^2, \\ \sigma_y &= \mu\left[\sum_{m=0}^{\infty} B_m S_{yd}^m(y) e^{i(\xi_m x-\omega t)} + \sum_{n=2}^{\infty} C_n S_{ye}^n(y) e^{i(\xi_n x-\omega t)}\right]\left(\frac{\pi}{2h}\right)^2, \\ \tau_{xy} &= \mu\left[\sum_{m=0}^{\infty} B_m T_{xyd}^m(y) e^{i(\xi_m x-\omega t)} + \sum_{n=2}^{\infty} C_n T_{xye}^n(y) e^{i(\xi_n x-\omega t)}\right]\left(\frac{\pi}{2h}\right)^2 \end{aligned} \tag{A.13}$$

with

$$\begin{aligned} S_{xd}^m &= -\left(\Omega^2 - 2m^2\right)\cos\left(\frac{\pi}{2} m \frac{y}{h}\right), \\ S_{xe}^n &= 2ink_n \cos\left(\frac{\pi}{2} n \frac{y}{h}\right), \\ S_{yd}^m &= -\left(\frac{v}{1-v}\Omega^2 + 2m^2\right)\cos\left(\frac{\pi}{2} m \frac{y}{h}\right), \\ S_{ye}^n &= -2ink_n \cos\left(\frac{\pi}{2} n \frac{y}{h}\right), \\ T_{xyd}^m &= -2imk_m \sin\left(\frac{\pi}{2} m \frac{y}{h}\right), \\ T_{xye}^n &= \left(\Omega^2 - 2n^2\right)\sin\left(\frac{\pi}{2} n \frac{y}{h}\right). \end{aligned} \tag{A.14}$$

Appendix B. Frequency map for a symmetric wave modes in a plate with sliding surfaces

See Fig. B.1.

References

Achenbach, J.D., 1973. Wave Propagation in Elastic Solids. North-Holland Publishing Company.

Babenkova, E., Kaplunov, J., 2005. Radiation conditions for a semi-infinite elastic strip. Proc. R. Soc. London A 461, 1163–1179.

Budreck, D.E., Rose, J.H., 1991. Elastodynamic completeness relations for scattered wavefields. SIAM J. Appl. Math. 51, 1568–1584.

Fraser, W.B., 1976. Orthogonality relation for the Rayleigh–Lamb modes of vibration of a plate. J. Acoust. Soc. Am. 59, 215–216.

Graff, K.F., 1975. Wave Motion in Elastic Solids. Clarendon Press, Oxford.

Gregory, R.D., Gladwell, I., 1983. The reflection of a symmetric Rayleigh–Lamb wave at the fixed or free edge of plate. J. Elast. 13, 185–206.

Gregory, R.D., Gladwell, I., 1984. The generation of waves in a semi-infinite plate by a smooth oscillating piston. J. Appl. Mech. (Trans. ASME) 51, 787–791.

Gregory, R.D., Gladwell, I., 1989. Axisymmetric waves in a semi-infinite elastic rod. Q. J. Mech. Appl. Math. 42, 327–337.

Karp, B., 2005. Dynamic version of Saint-Venant's principle – historical account and recent results. Nonlinear Anal. 63, e931–e942.

Karp, B., 2008. Generation of symmetric Lamb waves by non-uniform excitations. J. Sound Vib. 312 (1–2), 195–209.

Karp, B., 2009. Dynamic equivalence, self-equilibrated excitation and Saint-Venant's principle for an elastic strip. Int. J. Solids Struct. 46, 3068–3077.

Karp, B., Durban, D., 2005. Evanescent and propagating waves in prestretched hyperelastic plates. Int. J. Solids Struct. 42, 1613–1647.

Karp, B., Rittel, D., Durban, D., 2008. Health monitoring of joints using dynamic end effects. J. Sound Vib. 312 (1–2), 257–272.

Karp, B., Dorogoy, A., Wang, Z., 2009. Non-uniform impact excitation of a cylindrical bar. J. Sound Vib. 323, 757–771.
Miklowitz, J., 1978. The Theory of Elastic Waves and Waveguides. North-Holland Publishing Company, Amsterdam.
Mindlin, R.D., 1960. Waves and vibrations in isotropic, elastic plates. In: Goodier, J.N., Hoff, N.J. (Eds.), Structural Mechanics. Pergamon, New York.
Rose, J.L., 1999. Ultrasonic Waves in Solid Media. Cambridge University Press.
Torvik, P.J., 1967. Reflection of wave trains in semi-infinite plates. J. Acoust. Soc. Am. 41, 346–353.
Wijeyewickrema, A.C., Ushida, Y., Kayestha, P., 2008. Wave propagation in a prestressed compressible elastic layer with constrained boundaries. J. Mech. Mater. Struct. 10 (3), 1963–1976.
Zemanek Jr., J., 1972. An experimental and theoretical investigation of elastic wave propagation in a cylinder. J. Acoust. Soc. Am. 51, 265–283.